EGS Collab Project: Status, Tests, and Data

Kneafsey, T.J., Dobson P.F., Ajo-Franklin, J.B., Guglielmi, Y., and Valladao, C.A.
Lawrence Berkeley National Laboratory, Berkeley, California, USA
Blankenship, D.A., Schwering, P.C., and Knox, H.A.
Sandia National Laboratories, Albuquerque, New Mexico, USA
White, M.D., Johnson, T.C., Strickland, C.E., and Vermuel, V.R.
Pacific Northwest National Laboratory, Richland, Washington, USA
Morris, J.P., and Fu, P.
Lawrence Livermore National Laboratory, Livermore, California, USA
Mattson, E., Neupane, G.H., and Podgorney, R.K.
Idaho National Laboratory, Idaho Falls, Idaho, USA
Doe, T.W.
TDoeGeo, Redmond, Washington, USA
Huang, L., and Frash, L.P.
Los Alamos National Laboratory, Los Alamos, New Mexico, USA
Ghassemi, A.
University of Oklahoma, Norman, Oklahoma, USA
Roggenthen, W.
South Dakota School of Mines and Technology, Rapid City, South Dakota, USA

The EGS Collab team[1]

[1] J. Ajo-Franklin, S.J. Bauer, T. Baumgartner, K. Beckers, D. Blankenship, A. Bonneville, L. Boyd, S. Brown, S.T. Brown, J.A. Burghardt, T. Chen, Y. Chen, K. Condon, P.J. Cook, D. Crandall, P.F. Dobson, T. Doe, C.A. Doughty, D. Elsworth, J. Feldman, A. Foris, L.P. Frash, Z. Frone, P. Fu, K. Gao, A. Ghassemi, H. Gudmundsdottir, Y. Guglielmi, G. Guthrie, B. Haimson, A. Hawkins, J. Heise, M. Horn, R.N. Horne, J. Horner, M. Hu, H. Huang, L. Huang, K.J. Im, M. Ingraham, R.S. Jayne, T.C. Johnson, B. Johnston, S. Karra, K. Kim, D.K. King, T. Kneafsey, H. Knox, J. Knox, D. Kumar, K. Kutun, M. Lee, K. Li, R. Lopez, M. Maceira, P. Mackey, N. Makedonska, C.J. Marone, E. Mattson, M.W. McClure, J. McLennan, T. McLing, C. Medler, R.J. Mellors, E. Metcalfe, J. Miskimins, J. Moore, J.P. Morris, S. Nakagawa, G. Neupane, G. Newman, A. Nieto, C.M. Oldenburg, W. Pan, T. Paronish, R. Pawar, P. Petrov, B. Pietzyk, R. Podgorney, Y. Polsky, J. Popejoy S. Porse, B.Q. Roberts, M. Robertson, W. Roggenthen, J. Rutqvist, D. Rynders, H. Santos-Villalobos, M. Schoenball, P. Schwering, V. Sesetty, C.S. Sherman, A. Singh, M.M. Smith, H. Sone, F.A. Soom, C.E. Strickland, J. Su, D. Templeton, J.N. Thomle, C. Ulrich, N. Uzunlar, A. Vachaparampil, C.A. Valladao, W. Vandermeer, G. Vandine, D. Vardiman, V.R. Vermeul, J.L. Wagoner, H.F. Wang, J. Weers, J. White, M.D. White, P. Winterfeld, T. Wood, S. Workman, H. Wu, Y.S. Wu, Y. Wu, E.C. Yildirim, Y. Zhang, Y.Q. Zhang, J. Zhou, Q. Zhou, M.D. Zoback

ABSTRACT: The EGS (Enhanced Geothermal Systems) Collab project is performing stimulation and flow experiments in highly-monitored and well-characterized intermediate-scale (approximately10 to 20 meter) field test beds at a depth of approximately 1,500 meters in the Sanford Underground Research Facility (SURF) in the Black Hills of South Dakota. Our fracture stimulation and interwell flow tests are performed to better understand processes that control formation of effective subsurface heat exchangers that are critical to the development and success of EGS. Different EGS Collab stimulations will be performed under dissimilar stress conditions to produce data for model comparisons that better differentiate stimulation mechanisms and the evolution of permeability enhancement in crystalline rock. EGS Collab experiments provide a means of testing tools, concepts, and strategies that could later be employed under geothermal reservoir conditions at DOE's Frontier Observatory for Research in Geothermal Energy (FORGE) and other enhanced geothermal systems. Key to the project is using numerical simulations in the experiment design and interpretation of results, and the collection of high-quality stimulation/flow, thermal, geologic, and geophysical data. A wide range of geologic and geophysical data have been acquired and interpreted for pre-stimulation testbed characterization. Multiple stimulation and flow tests have been performed at SURF, and multiple data sets have been collected and analyzed during these tests including electrical resistance tomography, microseismic, continuous active source seismic monitoring, distributed temperature, and the SIMFIP tool has been used to identify fracture formation and characteristics. An overview of some of the numerical simulations and experiments performed at SURF are presented.

1. INTRODUCTION

Enhanced or engineered geothermal systems (EGS) resources in the western US could provide in excess of 500 GWe, significantly surpassing the resource base hosted by conventional hydrothermal systems (Williams et al., 2008) adding to the energy security of the United States. Over the entire United States, as much as ten times as much energy could be available based on an estimate using higher resource recovery factors (Augustine, 2016). These large potential resources are attractive to utilize, but there are significant technological challenges associated with developing this resource that need to be addressed. These include: (1) an incomplete understanding of techniques to effectively stimulate fractures in different rock types and under different stress conditions to communicate between multiple wells, (2) inability to image/monitor permeability enhancement and evolution at the reservoir scale at the resolution of individual fractures, (3) limited technologies for effective zonal isolation for multistage stimulations under EGS conditions, (4) lack of technologies to isolate zones for controlling fast flow paths and control early thermal breakthrough, and (5) lack of scientifically-based long-term EGS reservoir sustainability and management techniques.

To facilitate the success of FORGE and EGS, the DOE Geothermal Technologies Office (GTO) initiated the EGS Collab project (https://www.energy.gov/eere/geothermal/egs-collab). The EGS Collab project is utilizing readily accessible underground facilities to refine our understanding of rock mass response to stimulation at the intermediate scale (on the order of 10 m) for the validation of thermal-hydrological-mechanical-chemical (THMC) modeling approaches. Additionally, we are testing and improving conventional and novel field monitoring tools. The EGS Collab project focuses on understanding and predicting permeability enhancement and evolution in crystalline rock, including how to create sustained and distributed permeability for heat extraction from the reservoir by generating new fractures that complement existing fractures. The project is a collaborative multi-lab and university research endeavor bringing together a team of skilled and experienced researchers and engineers in the areas of subsurface process modeling, monitoring, and experimentation to focus on intermediate-scale EGS reservoir creation processes and related model validation in crystalline rock (Kneafsey et al., 2018a).

Three multi-test experiments are planned or in progress to increase understanding of 1) hydraulic fracturing (Experiment 1 - under way at the time of this writing), 2) shear stimulation in (Experiment 2 - starting soon), and 3) other stimulation methods (Experiment 3). Each Experiment is composed of a series of tests, and each test requires modeling to support design, and post-test modeling and analysis are performed to examine the effectiveness of our modeling tools and approaches. This process tests modeling and codes, allowing building confidence in and improve the array of modeling tools in use. Thermal circulation experiments to validate

predictions based on field data and stimulations are key to the project. So far in Experiment 1, we have performed several highly monitored hydraulic fracture stimulations, and will be proceeding to shear stimulation of natural fractures and fracture networks with increasing complexity. We have implemented a suite of rock/reservoir characterization methods potentially useful for EGS systems, as well as other methods available to improve understanding (Knox et al., 2017; Morris et al., 2018b), including microseismic monitoring, continuous active-source seismic monitoring (CASSM), electrical resistance tomography, and step-pressure and tracer tests. These help define the effective conducting surface area for heat exchange and determine the flow rate limitations for sustaining production well temperatures (Doe et al., 2014; Zhou et al., 2018). We are also developing new monitoring methods that are currently unable to work under geothermal reservoir conditions.

2. EGS COLLAB EXPERIMENT 1

Experiment 1 is being performed on the 4850 (feet deep) level at the Sanford Underground Research Facility (SURF) in Lead, South Dakota (Heise, 2015). This site (Figure 1) was selected as most suitable to effectively meet the needs of the first experiment based on an evaluation of a number of potential sites (Dobson et al., 2017). SURF is located in the former Homestake gold mine and is operated by the South Dakota Science and Technology Authority. It hosts a number of world-class physics experiments related to neutrinos and dark matter, as well as to geoscience research (Heise, 2015). As a former gold mine, SURF has been reasonably well characterized (Hart et al., 2014). Performing experiments in SURF offers a number of advantages to the EGS Collab project, including realistic in-situ stress conditions, cost-effective proximal monitoring of a deep crystalline rock mass before, during, and after stimulation through multiple boreholes drilled from an underground tunnel, infrastructure (e.g., ventilation, power, water and internet), and excellent staff dedicated to scientific research support (Dobson et al., 2017). The maximum temperature of the rock mass at the 4850 level is about 35°C, which is not optimal for a geothermal project. However, achieving realistic temperatures and stress would involve costly deep drilling and would not facilitate detailed characterization and monitoring, thus preventing us from achieving the EGS Collab objectives.

The objective of Experiment 1 is to establish a fracture network that connects an injection well and a production well using hydraulic fracturing. A schematic of the Experiment 1 testbed is shown in Figure 2. All holes for the experiment are nominally 60 meters long, drilled subhorizontally, and continuously cored. The test bed was envisioned to extend between injection and production holes (green and red lines in Figure 2), drilled in approximately the direction of the minimum principal stress based on prior characterizations in nearby rock conducted by the kISMET project (Oldenburg et al., 2017). This was done so that hydraulic fractures would tend to propagate orthogonally to the injection well. Six monitoring wells (yellow in Figure 2) were drilled and instrumented following characterization. Boreholes were characterized using optical and acoustic televiewers, full waveform seismic, electromagnetic properties, natural gamma, and temperature to the extent the characterization tools were available and functioning properly; the core samples were also studied to determine the nature and location of fractures. The test block surrounded by the monitoring boreholes was further characterized using seismic tomography (compressional- and shear-) using grouted and mobile sources and sensors (Daley et al., 2007; Linneman et al., 2018; Morris et al., 2018b; Schwering et al., 2018), electrical resistance tomography (ERT) for baseline (Johnson et al., 2019), and extended hydrologic characterization including tracer tests (Mattson et al., 2019). The detailed site characterization together with the array of installed monitoring systems and inversion methods helps to constrain the coupled process models. Sources and sensors have been grouted into the monitoring boreholes including: 1) passive seismic monitoring (Chen et al., 2018c; Huang et al., 2017; Newman and Petrov, 2018); 2) CASSM (Ajo-Franklin et al., 2011; Daley et al., 2007; Gao et al., 2018); 3) ERT in conjunction with dynamic electrical imaging using high contrast fluids (Johnson et al., 2014; Wu et al., 2018); 4) acoustic emissions (Zang et al., 2017); 5) distributed fiber optic sensors to monitor seismicity (DAS), temperature (DTS), and strain (DSS) changes (Daley et al., 2013). Additionally, during stimulation and flow testing we monitor fracture aperture strain using the Step-rate Injection Method for Fracture In-situ Properties (SIMFIP) tool (Guglielmi et al., 2015; Guglielmi et al., 2013); pressure and flow conditions in the injection and production boreholes; tracers when used (Zhou et al., 2018); and use wavefield imaging and inversion to help understand stimulation and flow behavior (Huang et al., 2017; Knox et al., 2016; Newman and Petrov, 2018). Laboratory measurements on selected core samples from the site measure fundamental physical rock properties needed constrain the coupled process models (Huang et al., 2017), complementing data available from kISMET (Oldenburg et al., 2017; Wang et al., 2017) and previous geotechnical studies at SURF. With the exception of very large data sets, all data collected and analyzed are kept on a data storage collaboration space (EGS Collab

Open EI site) in preparation for inclusion in DOE's Geothermal Data Repository (Weers et al., 2019).

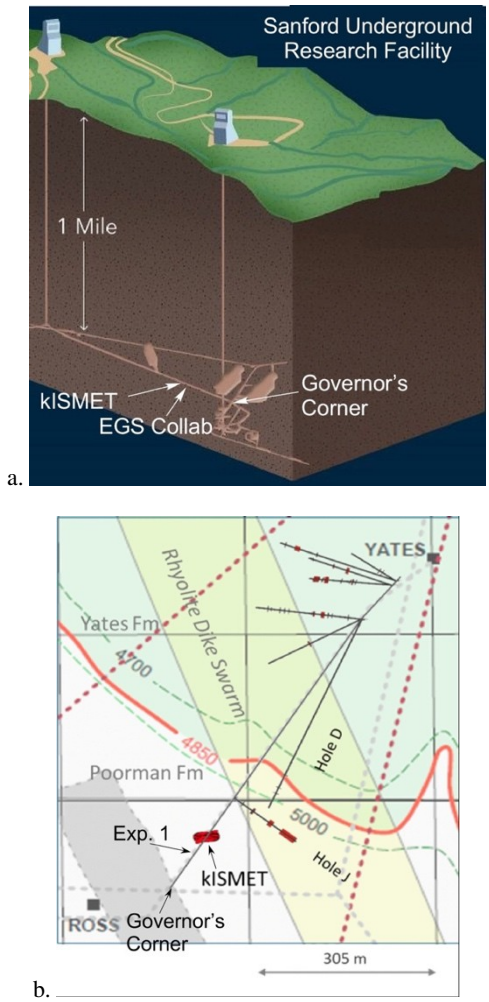

Figure 1: a) Schematic view of the Sanford Underground Research Facility (SURF), depicting a small fraction of the underground facilities including the Yates (left) and Ross (right) shafts, the 4850 level, the location of the kISMET experiment, and Experiment 1. b) Geologic map of the 4850 level of SURF in the vicinity of the site of Experiment 1. Both of these areas are located along the West Access Drift between the rhyolite dike swarms and Governor's Corner.

We have retrieved over 450 meters of core, which we have logged and photographed to identify foliation, veining, bedding, fractures, and variations in mineralogy. All of the boreholes are entirely within the Poorman Formation, a metasedimentary rock consisting of sericite-carbonate-quartz phyllite (the dominant rock type), biotite-quartz-carbonate phyllite, and graphitic quartz-sericite phyllite (Caddey et al., 1991). Carbonate minerals are calcite, dolomite, and ankerite. Other mineral phases (in addition to those listed above) include graphite and chlorite. The rock is highly deformed and contains veins consisting of carbonate, quartz, pyrrhotite, and minor pyrite. Optical and acoustic televiewer logs have identified natural fractures crossing the boreholes and these have been correlated with fractures mapped in the core samples. The adjacent kISMET boreholes previously used for stress measurement have been utilized to measure temperature gradients away from the drift walls. To the extent possible, all characterization data are being integrated into the geologic framework model of the Experiment 1 site.

Few fractures were encountered in the 300 m of vertical core collected at the kISMET site, so few were expected in the Experiment 1 test bed. We encountered many fractures however in the EGS Collab subhorizontal boreholes, and cores, core images, and borehole logging have been used to begin to understand the natural fractures in our test bed (see Common Discrete Fracture Network Model). Selected core segments from the test bed were sent to the National Energy Technology Laboratory (NETL) for measurements of X-ray computed tomography, magnetic susceptibility, gamma density, compressional wave velocity, Ca/Si, Ca/Al, Si/Al, and Fe/S ratios, abundance of light elements, Ca, and Si (Figure 3). In addition, cores have been sent out to researchers at a number of institutions to examine rock properties and behavior, and native biota.

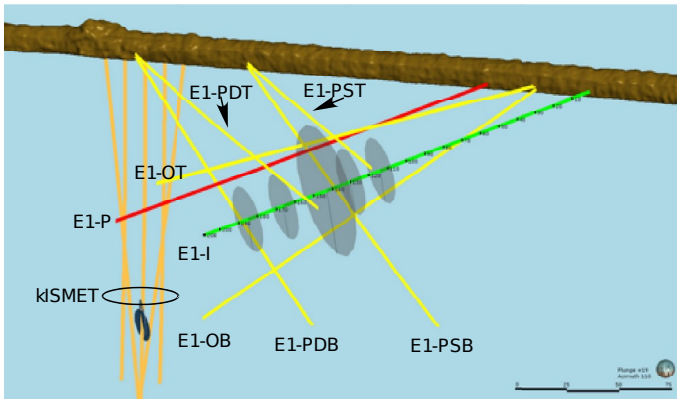

Figure 2: Ortho-view schematic of wells for Experiment 1 along the West Drift on the 4850 level of SURF. The green line represents the stimulation (Injection) well (E1-I), the red line represents the Production well (E1-P), yellow lines represent monitoring wells, and orange lines represent kISMET wells. Monitoring wells OT ("O" for orthogonal to the anticipated hydraulic fracture and "T" for top) and OB ("B" for bottom) originate between E1-I and E1-P, monitoring wells PST and PSB ("P" for parallel to the anticipated fracture plane, "S" is for shallow) originate midway down-drift, and monitoring wells PDT and PDB ("D" is for deep) originate near the kISMET boreholes. Orientation of stimulation and production boreholes is approximately parallel to S_{hmin}.

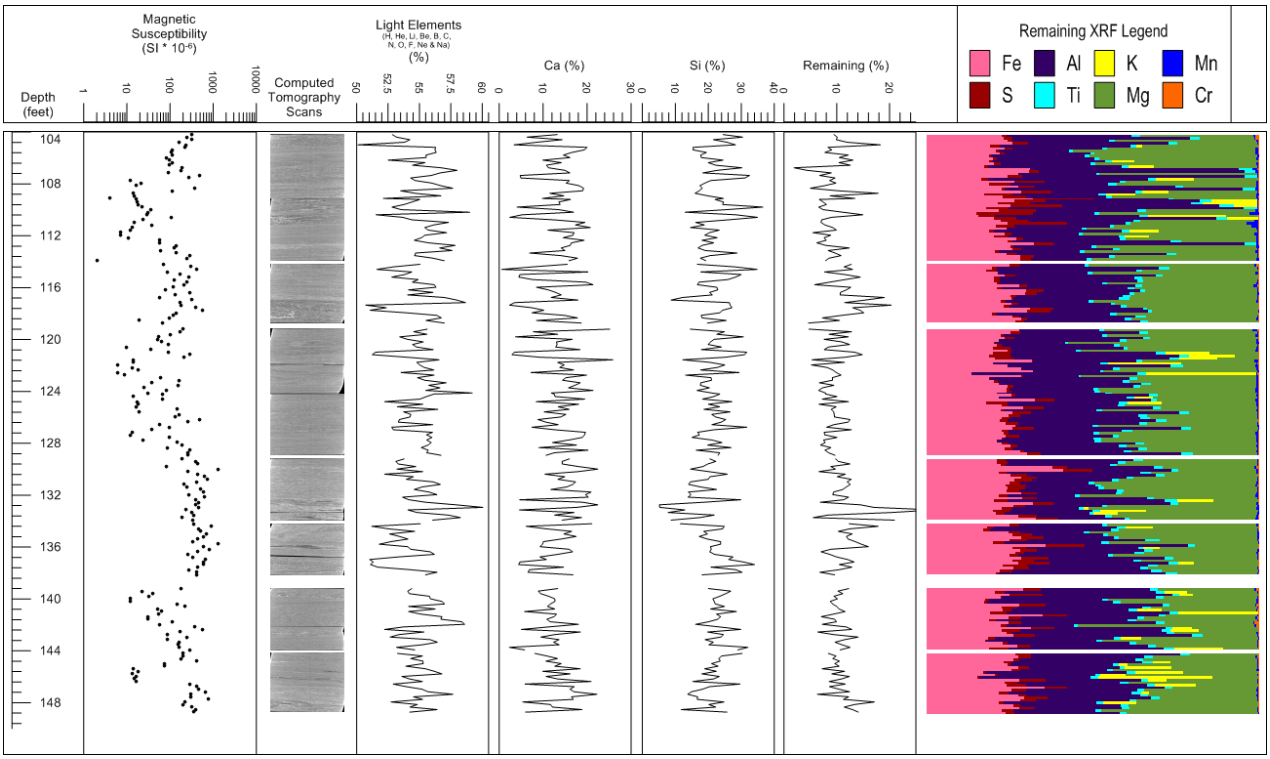

Figure 3. Some rock properties and variability from E1-I.

Stress measurements had already been performed adjacent to the Experiment 1 site as part of the kISMET project (Oldenburg et al., 2017). Based on a re-evaluation of kISMET data, the fractures generated from these tests indicate that S_{hmin} is about 21.7 MPa (3146 psi) and is oriented N-S (355 degrees azimuth) with a plunge slightly NNW at 9° (Kneafsey et al., 2018b). The vertical stress magnitude is estimated to be ~41.8 MPa (6062 psi) for the depth of testing (~1530 m), and the horizontal maximum stress is estimated to be 34.0 MPa (4931 psi) (Dobson et al., 2018).

2.1. ERT Characterization

The ERT characterization and monitoring system uses an array of electrodes grouted in place within the six monitoring wells, with 16 electrodes per well. The electrodes enable characterization of the 3D low-frequency electrical properties of the host rock, and changes in those properties during stimulation and tracer testing using both static and time-lapse ERT. Pre-stimulation baseline ERT images reveal the Experiment 1 testbed lies within a folded and dipping fabric of high and low electrical conductivity layers, likely associated with high graphite and/or sulfide mineralization and high quartz mineralization respectively (Figure 4). Baseline imaging results are consistent with borehole logs and core studies. Time-lapse imaging results to identify major flow paths during tracer studies are presented in Johnson et al., (2019).

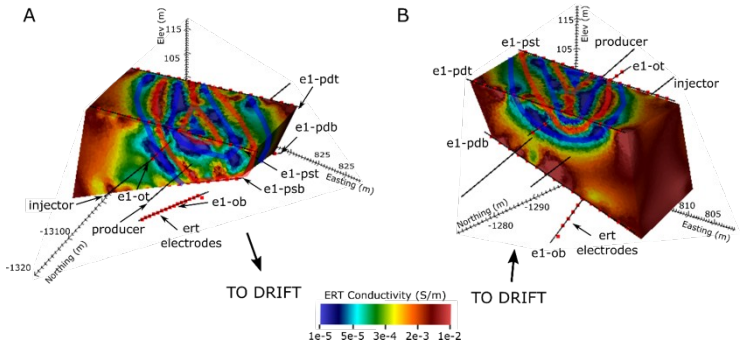

Figure 4. Pre-stimulation ERT images facing (A) away from and (B) toward drift. Red lines added to emphasize folded layering of high and low conductivity units revealed by ERT baseline.

2.2. Cross-borehole Seismic Characterization

A cross-borehole seismic campaign was conducted to develop 3-D seismic velocity models for the Experiment 1 test bed (Linneman et al., 2018). Active source seismic data were collected using an electrical sparker source and an electro-mechanical impulse source to generate compressional (P-) wave and shear (S-) wave energy, respectively, at varying depths in the stimulation and production boreholes. Seismic receivers were deployed in the production and injection wells (depending on which well was being used as a seismic source), in addition to receivers installed in the six monitoring wells to detect P- and S-wave arrivals. Raw data were assigned geometry and merged into shot gathers for arrival picking using Seismic Processing Workshop (SPW)

software by Parallel Geoscience Corporation. P-wave velocity (V_P) models were inverted using a Sandia code that exploits a 3D ray-based (eikonal) P-wave travel-time tomographic inversion methodology. After model convergence criteria are met, the output is a 3D V_P model (Figure 5). The model rock density was based on density measurements from rock cores (mean value of 2.764 g/cm^3).

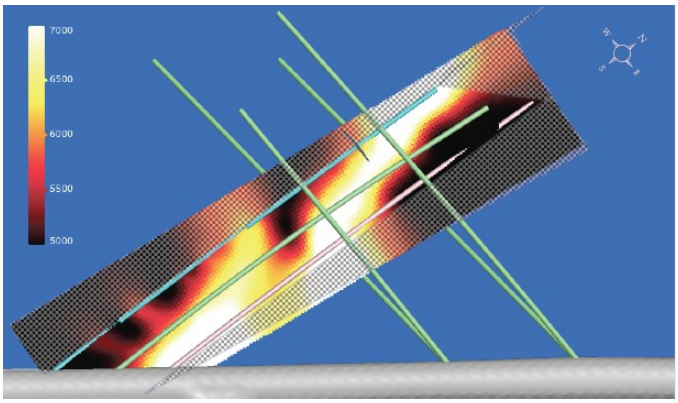

Figure 5. Slice of V_P model along the E1-I:E1-P plane. Velocities are in meters per second, with black denoting slowest velocities and white denoting fastest velocities.

3. STIMULATIONS

Initial analysis and modeling showed that fracturing using an inflatable packer system would likely result in fractures initiating parallel to the borehole rather than orthogonal the borehole (Abass et al., 1996; El Rabaa, 1989). To increase the likelihood of borehole-orthogonal fractures, notches were etched in the borehole walls using a custom notching tool built by Sandia based on simulations performed by LLNL (Morris et al., 2018b). These notches were placed based upon core and borehole logging data to avoid zones with prominent natural fractures and thus optimize fracture placement and orientation.

3.1. Stimulation Tests

Stimulations have been performed using a standard straddle packer modified by replacing the middle assembly by a modified Step-rate Injection Method for Fracture In-situ Properties (SIMFIP) tool (Figure 6), (Guglielmi et al., 2015; Guglielmi et al., 2013). The SIMFIP tool is designed to measure displacements between two clamped locations in a borehole. The stimulation system, described by Ingraham et al. (2018), uses multiple pumps including a Haskel pneumatic pump, a Quizix displacement pump, and a triplex pump providing a range of flow rates, pressures, and control precision choices. Combinations of these pumps and Teledyne ISCO high pressure syringe pumps are used to inflate and maintain packer pressure as well. The pumps and much of the system can be controlled from off-site allowing remote operation for many tasks. Additionally, the data can be viewed live remotely allowing test observation, discussion, and rapid feedback to the experimentalists, allowing rapid adjustment of operational parameters.

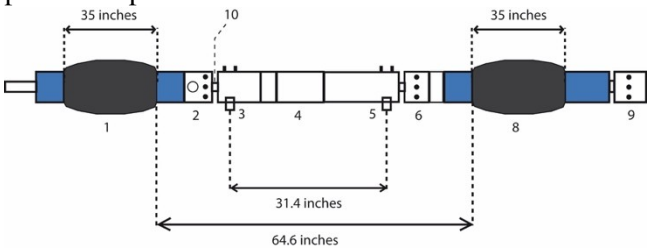

Figure 6. Typical straddle packer/SIMFIP assembly.

Four stimulation and flow tests have been performed as of February, 2019, resulting in many data sets and analyses (Chen et al., 2019; Frash et al., 2019; Fu et al., 2019; Huang et al., 2019; Johnson et al., 2019; Lu and Ghassemi, 2019; Mattson et al., 2019; Pan et al., 2019; Schoenball et al., 2019; Templeton et al., 2019; Weers et al., 2019; White et al., 2019; Winterfeld et al., 2019; Wu et al., 2019a; Wu et al., 2019b; Ye et al., 2019). The first stimulation attempt was performed at the 142' Notch (142 feet from the collar of E1-I). The packer interval is approximately 65 inches long including the SIMFIP tool (Figure 6), and a large apparently healed natural fracture was included in the interval. The stimulation was planned to occur in 3 steps. The initial stimulation was designed such that it might create an ideal 1.5 m penny-shaped fracture prior to being shut in for the night. The second step would extend the fracture to an ideal 5 m radius followed by being shut in for the night, and the third step would extend the fracture to the production borehole approximately 10 m away. Pressurizing at this location led to unexpected results including water flow returning up the borehole and a higher-than-expected fracture initiation pressure. Our analysis indicates that a hydraulic fracture was created with a breakdown pressure of 31 MPa (4500 psi), probably intersecting the observed natural fracture. A total of twelve liters of water were injected in this test. As shear stimulation was not intended in this test and the results indicated that we might be pumping into the natural fracture, the stimulation packer set was moved downhole to the 164' Notch and re-set to stimulate there.

The stimulation at the 164' Notch was carried out in steps over three days with shut-in periods between each step as planned for the 142'Notch. In the first step, 2.1 L of water was injected at a stable rate of 200 mL/min. The propagation pressure was 25.43 MPa (3688 psi) and the instantaneous shut-in pressure (ISIP) was 25.37 MPa (3679 psi). In the second step, 23.5 L of water was injected at 400 mL/min resulting in slightly higher propagation pressure and ISIP (25.95 and 25.82 MPa

respectively [3763 and 3744 psi]). The pressure decay following this step indicated that the hydraulic fracture may have intersected a natural fracture. The third step was performed at 5L/min and had an injection volume of 80.6 L, resulting in a propagation pressure and ISIP of 26.88 and 25.31 MPa (3898 psi and 3670 psi), and water being produced at E1-P. In addition to intersecting E1-P, this stimulation intersected the E1-OT monitoring well (located between the injection and production boreholes), as indicated by seismic sensors, a temperature increase measured by the DTS, and eventually water leaking out the top of the grouted E1-OT well. This intersection and leakage from this well has been problematic in subsequent testing.

The third stimulation was conducted at the 128' Notch, attempting to avoid a fracture that connects wells E1-OT and E1-P (the OT-P connector fracture system) while still connecting the injection and production wells. In this test, flow bypassed the top injection packer through fractures, and resulted in a hydraulic fracture connecting to E1-OT, but not E1-P.

After this stimulation, a medium-term set of hydraulic characterization tests was conducted at the 164' Notch (described below). Following that, a second stimulation experiment was completed at the 142' Notch by carefully placing the packer over regions of concern. This hydraulic stimulation experiment involved high flow rates and pressures, and extended the hydraulic fracture to E1-PDT, but not E1-PDB. Micro-seismic event locations (Schoenball et al., 2019) and the hydraulic fracture intersecting E1-PDT and not E1-PDB indicate that the fracture extended upward toward the drift. This was predicted by earlier modeling (Fu et al., 2018; White et al., 2018) of fracture growth under the stress gradient created by thermal cooling of the rock by the drift.

3.2. Fracture Displacements with SIMFIP

Figure 7 shows borehole displacements monitored with the SIMFIP probe during the second step of the stimulation at 164' Notch. Flow rate starts increasing with pressure at about 22 MPa (3184 psi), which can be interpreted as the pressure at which the fracture reopens created during the first step of the stimulation (Figure 7a - lower graph). Flow rate then exponentially increases with pressure up to the maximum fixed value of 400 mL/min. Below the reopening pressure, displacements show a linear variation with pressure that is interpreted as a reversible effect related to the system compressibility (Figure 7a, upper graph). At 18.6 MPa (2700 psi), borehole axial displacements start deviating from linearity, then followed by radial displacements at 23 MPa (3350 psi). This shows that some axial irreversible displacement initiates before a significant amount of radial displacement is triggered, and before a clear flow increase is observed. During shut in (dashed lines in Figure 7), both displacement curves display a different trend compared to the injection period. This trend is characterized by an initial linear decrease down to about 25 MPa (3619 psi) followed by a non-linear "diffusive-like" trend. Thus, the pressures coupled to the SIMFIP displacement variations give a refined estimation of the potential mechanisms triggered during this stimulation sequence, which is characterized by an initial traction parallel to the borehole axis followed at higher pressure and after some amount of water has been injected in the open fracture by the development of a large mixed axial-radial deformation.

Figures 7b and c show the irreversible displacements that initiate above 18.6 MPa (2700 psi). Displacements are in reasonable agreement with the opening of a N80-83E fracture almost perpendicular to the borehole axis until 23 MPa (3350 psi). Displacements slightly deviate from the borehole axis during this period, highlighting that fracture may initially open or reopen following a direction slightly oblique to the borehole's direction (which could relate to some local complex initiation on natural pre-existing borehole wall feature). Above 23 MPa (3350 psi), the measured radial displacement shows shear in addition to normal opening of the hydrofracture. Whether this radial signal is related to slip on the activated fracture plane or to stress drop induced by damage around the main fracture (as shown by the induced seismicity swarm) are key questions that will require additional analyses of the signals. During the shut in period, mainly displacement normal to the average fracture plane is observed, and an apparent complete closing is measured. Again this could mean that the shear component is related to stress drop caused by shear-induced failure in the environment of the hydrofracture.

Figures 7b and c also allow a first estimation of the fracture opening during the stimulation, of about 200 to 230 microns. The SIMFIP data allow tracking the evolution of the stimulated fracture aperture (thus estimating how efficient the stimulation is), and highlight an unexpected significant borehole radial deformation component given the initial concept which drove the design of this experiment, of the borehole being almost parallel to the minimum principal stress. This could mean that either the stress tensor is not exactly oriented as expected or that damage-induced shear stress release around the growing fracture and produced this apparent shearing of the borehole.

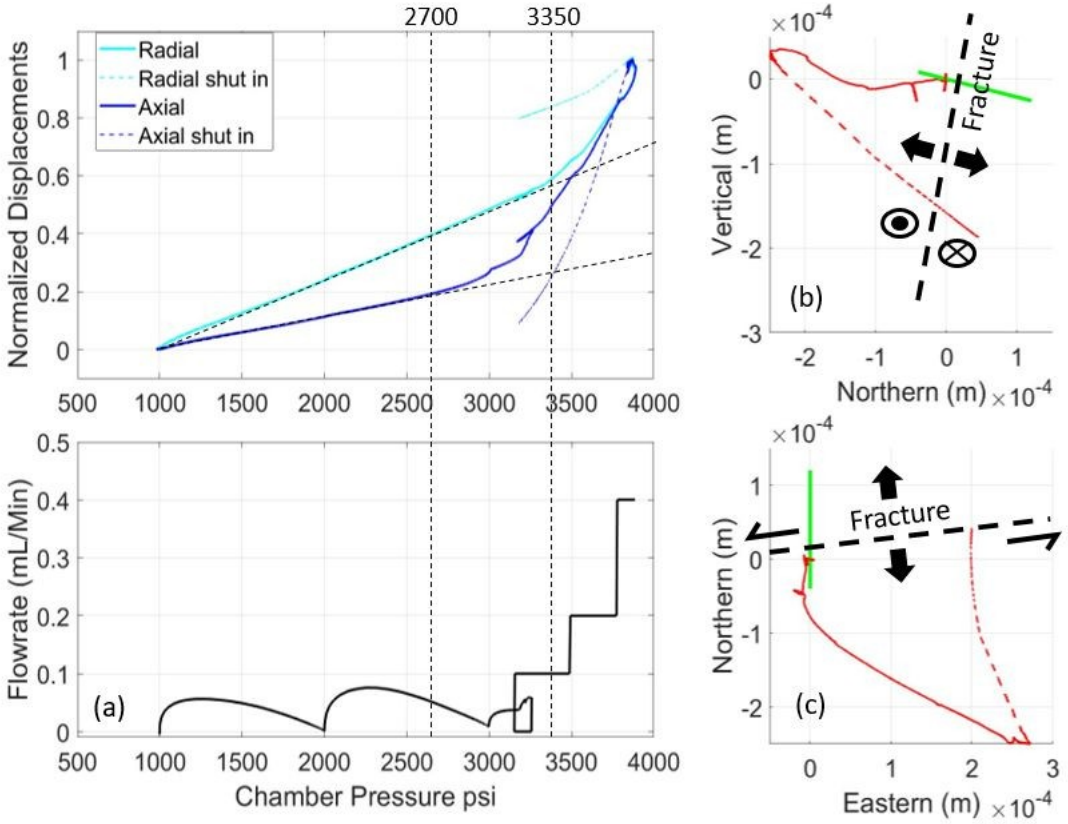

Figure 7: SIMFIP displacements during the second step of the stimulation at 164' Notch; (a) Lower graph shows the flow rate increase with pressure applied in the straddled interval and the upper graph shows the axial and radial displacements vs pressure; (b) Vertical-vs-North Displacement variations and (c) North-vs-East displacements (green line figures the borehole dipping 12°North and dashed line is the average orientation of the stimulated fracture).

3.3. Microseismicity

Microseismic monitoring has been performed throughout the repeated stimulation experiments and subsequent flow tests using a dense 3D sensor array including two cemented hydrophone strings with 12 1-component sensors at 1.75 m spacing accompanied by 18 3-component accelerometers, deployed in the 6 monitoring boreholes, completely encompassing the stimulation region. Continuous records were obtained using a novel dual recording system consisting of a conventional 96-channel exploration seismograph and a high-performance 64-channel digitizer sampling sensors at 4 and 100 kHz respectively. We detected thousands of microseismic events with recorded energy generally between 3 kHz and 40 kHz using a standard STA/LTA (ratios of short-time averages and long-time averages) detector. The locations of these events are consistent with creation of a hydraulic fracture and additional reactivation of pre-existing structures. Using manual pick refinement and double-difference relocation we are able to track the fracture growth with high precision (Figure 8a). We estimate the times and locations of the fracture intersecting monitoring and production boreholes using microseismic events. Our results are in excellent agreement with independent measurements using distributed temperature sensing, in-situ strain observations and measurements of conductivity changes (Schoenball et al., 2019).

Additional detection and location using a novel cross-correlation method based on synthetic and recorded STA/LTA ratios larger than 0.7 from microearthquake data recorded from May to July, 2018, show that the events are located along the created fractures and existing fractures. Figure 8b shows some of the approximately 5,500 events with correlation coefficients of synthetic and recorded STA/LTA larger than 0.6 that were identified over this duration (Chen et al., 2019). Microseismic events have also been segregated into cluster and non-cluster events based on waveform cross-correlation values (Templeton et al., 2019). Events that are part of a cluster indicate a higher degree of waveform similarity with at least one other event. This could be an indication of similar source mechanisms due to multiple ruptures of the same asperity on the same fracture slip patch (Figure 8c).

Fu et al. (2019) analyzedmicroseismic events from five stimulation "episodes". Approximately 400 microseismic events were located within the specific time windows. Analysis indicates a number of things including; 1) OT-P connector - an open natural fracture

with large aperture to the east of the injection well - apparently hindered fracture propagation but does not completely prevent the eastward propagation of the microseismic cloud (a later stimulation using a greater injection volume produced substantial microseismic events to the east of OT-P connector towards the end of injection; 2) the microseismic cloud from the five stimulations indicate a planar, largely vertical structure; 3) this fracture plane to the west of OT-P connector is comprised of two distinct, relatively small parallel planar features; 4) on the inferred fracture plane to the west of OT-P connector, seismic event clusters from different stimulation episodes seem to rarely overlap, suggesting different areas on the plane were seismically "activated" by different stimulations. An area that had been activated by a prior stimulation tends to be seismically "silent" in subsequent stimulations. This suggests the microseismic events are associated with the creation of a new fracture surface.

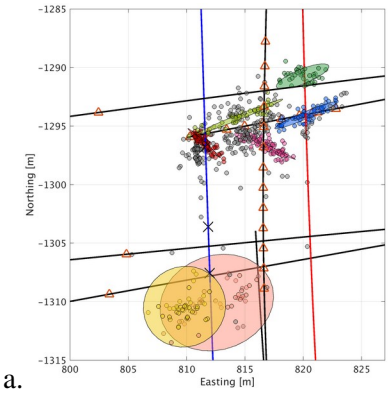

a.

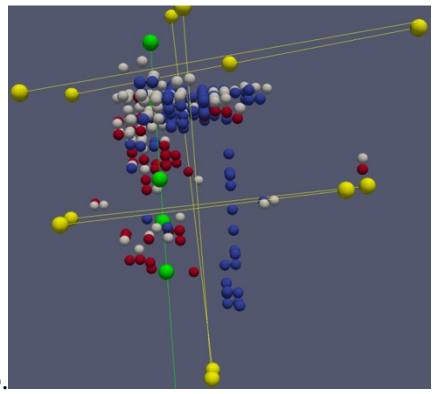

b.

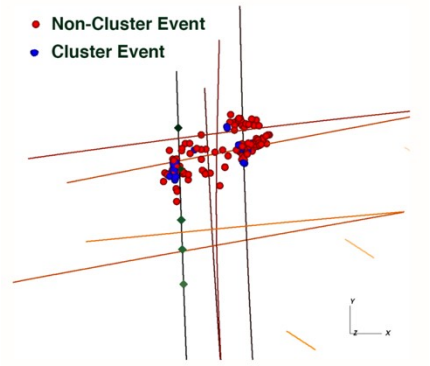

c.

Figure 8. a. Map view of located seismic events and fracture planes inferred from these data. b. STA/LTA ratio events larger than 0.7 from microearthquake data recorded from May to July, 2018, showing that the events are located along the created fractures and existing fractures. c. Map view showing results from a cross-correlation cluster analysis of seismic events that occurred in June 2018. Blue circles indicate events that correlate with at least one other event above a 0.5 cross-correlation threshold. Events that are not linked above the threshold are in red.

3.4. CASSM Results and Interpretation

The continuous active-source seismic monitoring system was also deployed at the testbed. The CASSM experiment involved the repeated activation of a sequence of small piezoelectric sources (4" length, 17 sources), recorded by the permanent monitoring array, to allow imaging of seismic property changes within the stimulated regions. The key imaging targets beyond the

new fracture network were aseismic property variations, mainly changes in fracture aperture due to injection pressure as well as fracture closure & healing. Data quality was excellent with source energy recorded to 24 kHz on both receiver arrays. The data were first processed for differential P-wave traveltime tomography using (a) an initial filtering stage, (b) a manual pick of the baseline dataset, (c) followed by cross-correlation based differential delay estimation. The resulting traveltime differences were inverted using a hybrid L1/L2 tomography code. Figure 9 (top) shows the P-wave velocity reduction in the plane between E1-OT and E1-OB immediately after the "drive to production" stage of Stimulation 2. As can be seen, the zone of velocity reduction aligns with the primary fracture as determined by microseismic analysis (red circles) as well as the DTS hot spots detected in well OT. The velocity anomaly also decreased in magnitude during the shut-in of the injector, suggesting that the technique has sensitivity to the stress state on the fracture.

Beyond transmission tomography, the scattered wavefield was also evaluated for fracture imaging (Gao et al., 2018). Initially, 3D anisotropic full-waveform inversion was applied to the CASSM data to improve the seismic velocity model. Then, 3D least-squares reverse-time migration was applied for the anisotropic medium to the CASSM data to produce high-resolution images. Figure 9 (bottom) shows an example of a fracture forming at the 164' Notch during the first stimulation (Pan et al., 2019).

4. HYDRAULIC CHARACTERIZATION

Three series of hydraulic characterization tests have been conducted as of January, 2019; two at the 164' Notch and one at the 142' Notch. Prior to the hydraulic characterization and following the stimulation where water flowed out of the OT monitoring well, grout was added to the top 6.1 m (20 ft) of the E1-OT borehole. This top portion was not initially grouted when the bottom part was, and the hope was to reduce flow out of the well and improve the connection between E1-I and E1-P.

4.1. Flow Tests

The stimulation and flow system was designed to allow remote operation under ideal conditions (Ingraham et al., 2018; Knox et al., 2017). Tests have been performed lasting nearly a month, with little hands-on adjustment required. This feature has proved to be very valuable in that is can allow long-term operation from more comfortable quarters.

The first hydraulic characterization tests were pressure transient tests performed in both E1-I and E1-P at low flow rates (i.e., ≤ 20 ml/min). Peak pressures during these tests (18.1 MPa, 2630 psi) for E1-I and 20.7 MPa (3000 psi) for E1-P stayed below fracture propagation pressure. During these tests, flows were noted from the collars of E1-OT and E1-PST. In the second test, a series of increasing pressures were applied in E1-I. In the first of these tests flow from E1-P declined sharply, and flow from E1-PSB increased. This possibly indicates that the hydraulic fracture connects to the OT-P connector fracture system. High flow rates (i.e., up to 4 L/min) and pressures (i.e., 30.0 MPa or 4355 psi) exceeding the fracture extension pressure were applied in the final hydraulic characterizations test at the 164' Notch. Maximum flows were 0.4 L/min from E1-P and 0.2 L/min

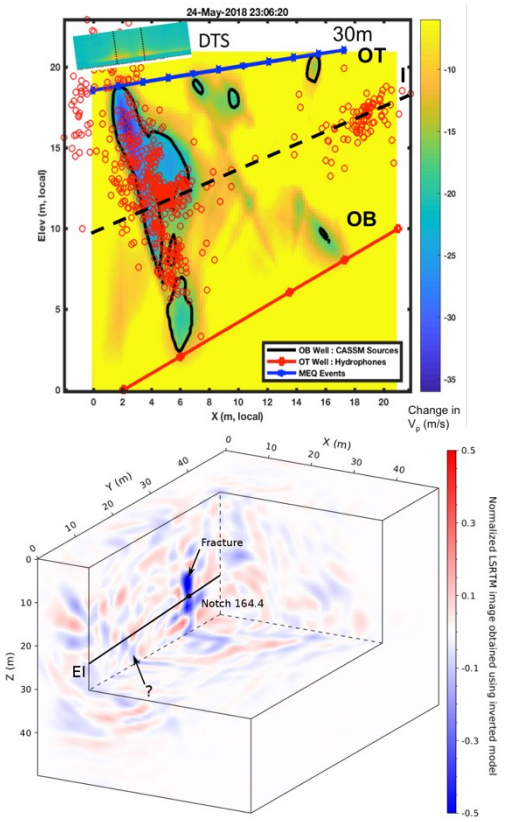

Figure 9: top - CASSM traveltime tomography (colormap) results compared to MEQ hypocenters (red circles) projected into the imaging plane. The tomogram shown is for the time immediately after maximum injection pressure during the "drive to production phase of stimulation 2. bottom - Least-squares reverse-time migration of CASSM data acquired using hydrophones and accelerometers at 22:29:19 and 22:47:47 on 5/24/2018 and anisotropic elastic-waveform inversion results, revealing the fracture created by hydraulic stimulation 2, and some other possible existing fractures. The image of the created fracture matches with the location of the notch at 164.4ft.

from E1-OT, reaching 60% recovery at times. The flows from E1-PST and E1-PSB remained small (i.e., 2.3 ml/min and 5.2 ml/min, respectively). At the end of the test, sufficient pressure built up beneath the bottom of injection packer in E1-I resulting in an upward

displacement of the packer and SIMFIP assembly. This indicates that the OT-P connector fracture system extends toward the bottom of E1-I.

The intermediate-rate flow test at the 164' Notch required higher-than-expected pressures to maintain the 0.4 L/min flow rate (29.3 MPa, 4250 psi). With the production packer interval set to span the anticipated hydraulic fracture location, water was initially produced from E1-OT and from E1-P from the zone above the top packer. To locate the inflow location, several E1-P packer locations were investigated: 1) shifting up 1.2 m (4 ft), 2) up1.8 m (6 ft), and 3) up 2.4 m (8 ft). After moving up 1.8 m., no flow was observed from E1-P. In the final location flow was recorded from below the packed interval. Between the first and second packer assembly shifts, the upper packer was independently deflated, and flow was observed from above the packers, indicating the upper packer was previously set over the OT-P connector intersection. This indicates that flow was preferentially entering E1-P via the OT-P connector fracture system instead of the hydraulic fracture.

The second hydraulic characterization test from the 164' Notch was performed to investigate the test bed under sustained flow conditions, emphasizing ERT to characterize the fracture network (Johnson et al., 2019). At the same time, a series of conservative and sorbing tracer experiments were conducted (see discussion below and Mattson et al., 2019). Prior to this test, the top of the E1-OT monitoring well was sealed with epoxy to increase the flow resistance into the drift. Initial injection flow rates were maintained at 0.4 L/min, and injection pressures held approximately steady near 28.3 MPa (4100 psi) (Figure 10). While flow conditions were approximately steady, DNA and C-Dot tracers were injected and recovered. Outflow was recorded from three regions in E1-P - below the packed interval, within the packed interval, and above the packed interval, and from E1-OT, E1-OB, and E1-PST. After some time, the volumetric percent recovery of the injected water approached as high as 84%. New leak points appeared as well, including from rock bolts that anchor the wire mesh support structure of the drift. After roughly steady conditions for 7 days, the pressure required to inject 0.4 L/m started to increase. Short-duration high-flowrate flushes were performed to halt the pressure increase, each time resulting in lower pressure required to maintain the 0.4 L/m flowrate. Following each, however, pressure steadily increased at a rate of about 115 kPa/hr (16.7 psi/hr). We changed to steady pressure injection at 29.0 MPa (4200 psi), which resulted in reducing flow rates over time. Several other changes were made to attempt to return the system to its earlier steady state including switching from mine water (similar to tap water) to deionized and then softened water, adding bromine biocide, and chilling the injection water. Each significantly affected the flow, however not always consistently and the pressure increase ultimately occurred again. Chilling the water by 10 to 15°C resulted in a pressure drop of 1 MPa (150 psi) within hours of the temperature change with a steady injection rate of 0.4 L/min. Within 36 hours of steady-rate pumping, however, the injection pressure started to rise again rapidly, with a concurrent drop in the recovery of water from the producing boreholes, which had principally become E1-OT. The injection pressure increased to a selected threshold of 31 MPa (4500 psi), at which point pressure control was applied and the injection rate declined significantly and the test was halted.

The third characterization test was at the 142' Notch following the hydraulic stimulation there. A sewer camera was deployed to identify fluid entry points into E1-P, which had been dewatered earlier allowing easy visualization of inflow into the borehole. Flow rates ranging from 0.4 L/m to 4 L/m were applied over different durations. The initial flow rate of 0.4 L/min yielded an injection pressure of 22.8 MPa (3300 psi). Flows were observed from multiple locations including E1-OB and E1-P, and minor drips from the drift ceiling, indicating that the stimulation had extended beyond E1-P, intersecting the OT-P connector natural fracture system. The injection pressure required to inject at 2.0 L/min was 32.4 MPa (4700 psi), near the fracture extension pressure. Not surprisingly, flows were observed from E1-OB, E1-P, E1-PST, and E1-PSB. At 4.0 L/min injection rate for durations of 70 and 22 minutes, the injection pressure showed only slight initial increases, then declined, typical of fracture extension. Flow from E1-OB increased over the experiment from less than 0.01 to 0.4 L/min. Visualization in E1-P using the sewer camera identified water coming in six jets and one slit. These appeared to be in two clusters, approximately 0.2 m (0.7 ft) apart, near the 30.5 m (100 ft) depth in E1-P. Whereas the mechanisms may be different, it should be noted that two clusters of jets, separated by a small distance, were also found in E1-P from the hydraulic stimulation at the 164' Notch, and in both cases the location of the inflow to E1-P was near where one would predict a hydraulic fracture to extend based on the stress orientation.

4.2. Impact of Leak at Monitoring Wells E1-OT and E1-OB and Well Repair

Early modeling and analysis indicated that the presence of a low-pressure boundary such as at an open borehole would drain that region of the fracture, reducing the propensity of the fracture to continue (Frash et al., 2018a; Frash et al., 2018b; Morris et al., 2018b). Thus, leaking monitoring wells are likely to influence the extent of the created fracture, tending to limit the

extension particularly in the neighborhood of the leaks. The depth of the well/fracture intersection can easily be determined using the DTS and passive seismic monitoring. Temperature changes observed using DTS possibly resulting from the Joule-Thomson effect under depressurization cause warming of the water (Zhang et al., 2018a). The magnitude of the temperature change indicates that the water entering the borehole experiences a significant pressure drop, however that pressure drop has not been quantified.

Significant effort has been expended to repair the monitoring boreholes that have significant leaks. For well E1-OT, the well was initially incompletely grouted leaving 6 meters of open hole (roughly corresponding to the cased interval). Grouting was completed following the initial stimulation, while leaving a tube to allow further pressure grouting. Upon additional leakage through the conveyance tube, the pressure-grouting tube, and other locations in the well, a very low viscosity epoxy was used to fill gaps under a low hydraulic head. This was partially successful, however it broke again when a high-flow high-pressure flow test was performed. Both the E1-OT and E1-OB wells have now experienced significant leaks from different stimulations. Custom well caps allowing feedthrough of the wires and fibers have been attached to matching welded flanges. These pressure-tight caps were used to apply low-viscosity epoxy at high pressure to help seal the monitoring wells.

4.3. System Characterization using Tracers

Ten tracer tests have been conducted to characterize flow pathways during the second hydraulic characterization test for 164' Notch (October 24th to November 20th, 2018) during steady state injection of 400 ml/min at the injection well (Mattson et al., 2019). Injected tracers include DNA, C-Dots (fluorescein nanoparticles), fluorescein, rhodamine-B, sodium chloride, lithium bromide and cesium iodide: several incidental tracers include varied injected water chemistry (mine water, softened mine water, deionized water). The tracers have been detected in three wells (leaking monitoring wells and the production well) located about 7.5 to 10 meters away from the injection interval. The tracer breakthrough curves from these locations have been adjusted to account for the

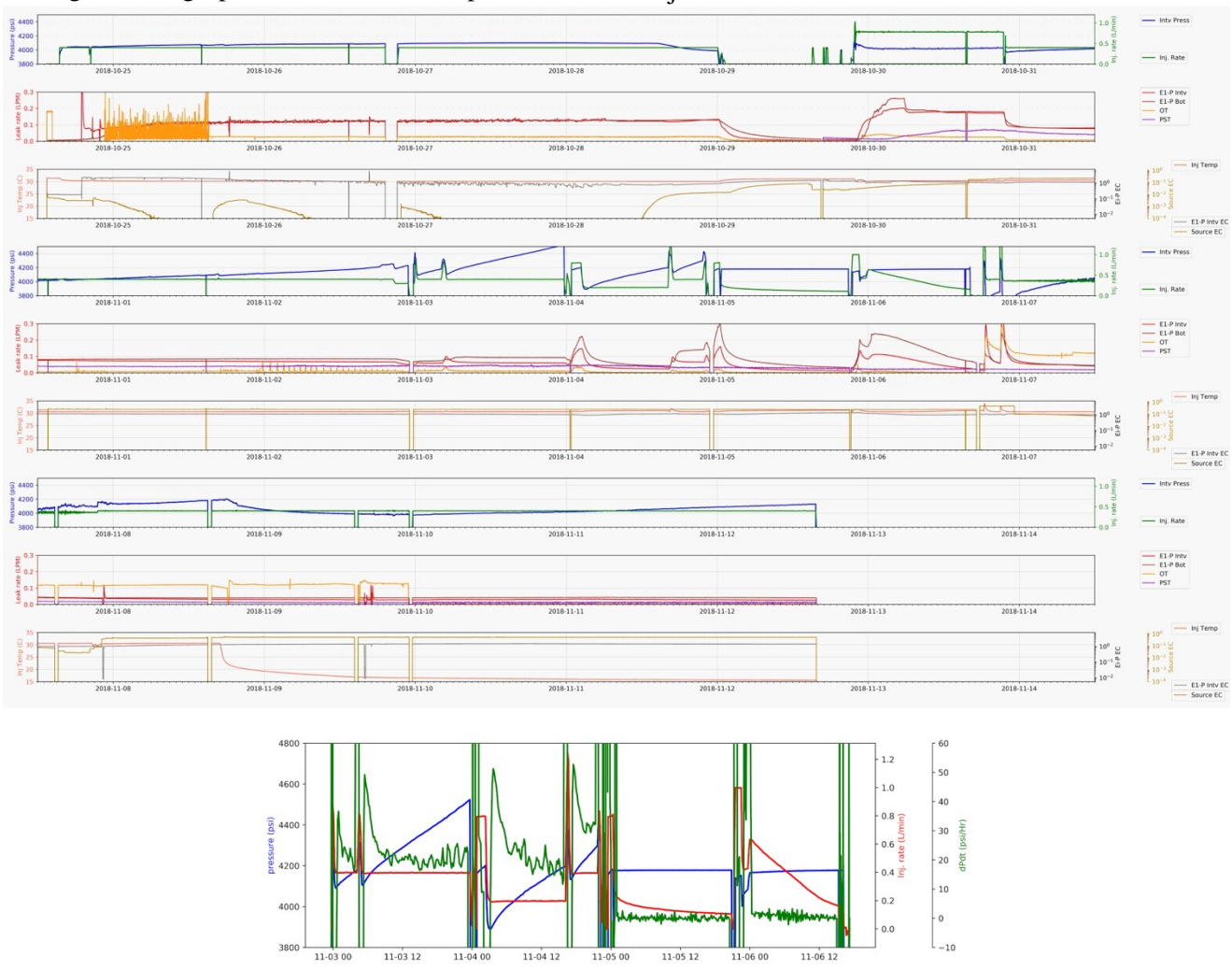

Figure 10. Summary of data from the second hydraulic characterization test at the 164' Notch. All dates and time are in UTC. The first, fourth, and seventh panels from the top show the injection pressure and injection rate; the second, fifth, and eighth panels

show the out-flow rates from different wells and two isolated segments in well E1-P; the third, sixth, and ninth panels show the injection fluid temperature and the electrical conductivity (EC) of the source water and the water from well E1-P. The bottom plot highlights the dp/dt evolution during one of the more interesting periods.

residence time in the injection and production tubing (e.g. Figure 11). Data analysis is ongoing, however, data for fluorescent C-Dots, rhodamine-B, and chloride have been analyzed for concentration vs. time/volume at the production wells. Changes in tracer breakthrough are correlated with stimulation events. Results from early testing have been re-analyzed considering the amount and location of injected water recovery and the mass of tracer recovered. Field results indicate tracer breakthrough; it occurred more quickly than predicted by simple numerical models. Additional analyses and extension to heat transfer have also been performed (Zhang et al., 2018b), and code to better analyze tracer tests have been improved (Winterfeld et al., 2019).

In addition to standard analysis of tracer data, the feasibility of inferring fracture flow patterns in Experiment 1 is being evaluated through stochastic modeling of tracer tests (Wu et al., 2019a). This uses a fracture model with connected hydraulic and natural fractures based on applicable field data, including core logs, seismic events, DTS, and flow measurements, and includes an injection well, a production well and multiple monitoring wells according to the experiment design. A brute-force, Monte Carlo approach is used to perform massive realizations to simulate tracer transport processes in the hydraulic and natural fractures, and tracer breakthrough curves at multiple monitoring wells are obtained for each realization. A fitting criterion is then employed to select viable realizations that yield optimal fits of the measured tracer breakthrough curves, and fracture flow patterns in the hydraulic and natural fractures are analyzed through these selected realizations.

5. NUMERICAL STUDIES

Validation and improving numerical modeling tools are primary goals of the EGS Collab project. In addition to the simulations and analyses already mentioned, a large number of modeling studies have been conducted for a variety of reasons, providing feedback for design, and interpretation of results (White et al., 2019). Initial modeling efforts (Chen et al., 2018a; Chen et al., 2018b; c; Fu et al., 2018; Gao et al., 2018; Huang et al., 2017; Knox et al., 2017; Mattson et al., 2018; Morris et al., 2018a; Morris et al., 2018b; White et al., 2017; White et al., 2018; Zhang et al., 2018a; Zhou et al., 2018) have focused on several initial questions to guide experiment design including 1) preferred orientation for the stimulation borehole, 2) anticipated number and magnitudes of seismic events during hydraulic stimulation, 3) flow rates and pressures for the circulation experiments to prevent fracture propagation, 4) circulation duration required to achieve measurable temperature changes in the production borehole, 5) the role of the production well in preventing fracture propagation to the drift, 6) the orientation of a hydraulic fracture from the unaltered or notched injection borehole drilled in the direction of the minimum principal stress, 7) the impact of notch geometry on stimulation pressure and near wellbore impedance, 8) effect of the thermal profile on the stresses around the drift, 9) the alteration of the stress state in the experimental volume via mechanical and thermal alteration from the mine workings and drift cooling, and 10) anticipated shape and arrival time in terms of injected fluid volume of the hydraulically generated fracture under the mechanically and thermally altered stress state. Current modeling studies (White et al., 2019) are focused on (for example) modeling stimulation in fractured domains and mixed-mode stimulation, tortuosity dominated, and natural fracture networks, tracer breakthrough curves and implications thereof (Wu et al., 2019a), tracer return and implications, better understanding the thermal environment around the drift, thermal signatures from flow tests, and discrete fracture network modeling. Mechanistic modeling to interpret stimulation data and better understand fracturing behaviors has been performed using a series of 2D and 3D simulations. These simulations use coupled conjugate network flow and quasi-static discrete element model (DEM). The fracturing behaviors of naturally fractured crystalline rocks under hydraulic stimulations are investigated by systematically varying geometrical, hydraulic and mechanical attributes of natural fractures (Huang et al., 2019).

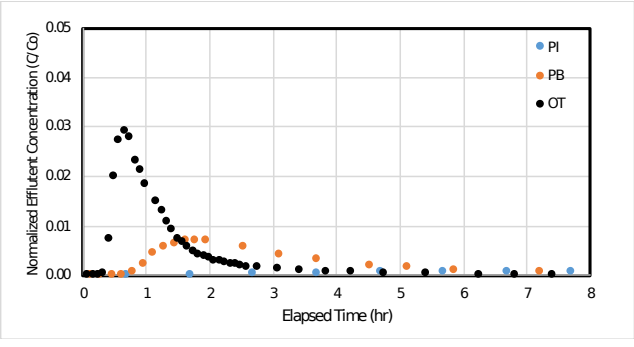

Figure 11. Example of the C-Dot tracer breakthrough curves for three locations for the November 14 tests. “PI” indicates the interval in the production well, “PB” indicates the zone below the packer in the production well, and “OT” indicates water collected from the leaking OT well.

6. COMMON DISCRETE FRACTURE NETWORK MODEL

We have developed and are using a geologic framework model using Leapfrog (Seequent Limited). Data incorporated includes recently obtained measurements from this project, geologic data contained in the Maptek Vulcan database for SURF (e.g., Hart et al., 2014), available geotechnical reports, and results from the kISMET study (Oldenburg et al., 2017). From this we created three scales of geologic models: a mine scale model, an intermediate scale model that includes multiple drift levels, and a more detailed model that encompasses the immediate area around Experiment 1 for visualization and simulation. Additional geologic information is included in the models as it becomes available. The geologic framework model is important in constraining the grid block properties for the coupled process models simulating the EGS Collab experiments, visualization, and providing a more uniform basis for model comparison.

With regards to natural groundwater flow, the scarcity of flowing fractures in the DUSEL characterization program and the lack of conductive fractures in the kISMET program (Oldenburg et al., 2017) created an expectation that the Collab site, which is very close to kISMET, would lack hydraulically conductive fractures. As work proceeded, several findings indicated that conductive fractures might be present (e.g., Roggenthen et al., 2018; Ulrich et al., 2018).

First, geologic mapping of the drift walls identified one 3-m thick fracture zone characterized by higher fracture intensity, open fractures sometimes with crystal linings, and local vuggy porosity. This “weep zone” has small water flows at the drift wall that appear as evaporative crusts and small drips. The weep zone does not cross the central portion of the Collab block, defined as the volume within the monitoring hole array.

The second indicator of conducting fractures was an observation of cross flow between boreholes during drilling. The discovery of this feature triggered an investigation to identify conductive fractures. The approach involved a cross hole survey injecting wells at the pressure of the mine water system and observing flows in other holes using a downhole video camera. The survey revealed a significant conducting fracture connecting the production well, EI-P, and the upper north-south monitoring hole, E1-OT. An integration of the flow survey results with core and borehole televiewer data identified a single open fracture striking NNW with a near vertical dip, which was named the OT-P Connector. This fracture does cross the central portion of the array, and later observations of seepage on the drift walls during injections from E1-I suggest that the OT-P Connector might capture some of the flow from stimulation.

The third flow indicator was a naturally flowing fracture in one observation borehole (EI-PST). The fracture initially flowed at about 1 liter per minute, dropping over a month to about 0.7 liters per minute, and then ceasing flow altogether. Televiewer logs and the conductive fracture survey identified the location and orientation of this fracture. It aligns with the OT-P Connector and may be the same feature.

When it became clear that natural fractures were likely to be influencing the stimulations, a comprehensive study of all the natural fracture observations including borehole logs, core, and flow indicators was used to create a common discrete fracture network model or CDFNM (Figure 12) (Schwering et al., 2018). The model was compiled for visualization in Golder Associate’s commercial DFN software, FracMan to serve as a database for the project’s modeling teams.

7. LABORATORY STUDIES AND DIRECT OBSERVATIONS

Laboratory studies are also under way to support understanding of the stimulations and rock behavior in Experiment 1. At Stanford University, six unique synthetic DNA tracers were prepared for running at the SURF site. Laboratory tests evaluated the use of the DNA tracers in combinations. These tests showed that the tracers were distinguishable from each other, allowing simultaneous or sequential use. Friction-stability-permeability measurements have been performed at Penn State University to examine the response of permeability evolution to stability (Yildirim et al., 2018). Also, a velocity stepping test has been performed to show the key role of velocity changes in permeability. Schist is frictionally weak ($\mu<0.5$) and exhibits velocity-strengthening behavior. Permeability declines during sliding and permeability reduction decreases with the accumulation of displacement. Wear products of low surface roughness fractures may seal transmissive fluid channels, explaining the observation.

The variability of rock strength and elastic properties from core samples from the Experiment 1 stimulation volume are being quantified at the University of Wisconsin (Condon et al., 2018). The unconfined/uniaxial compressive strength varied widely and is weakest for foliation orientations of 45 and 60 degrees as measured from the normal of the foliation plane to the sample axis. Young's modulus under confined conditions that are representative of the in-situ stress also varied widely. Ultrasonic P-wave velocities varied sinusoidally as a function of foliation orientation. Fracture toughness measurements are also being performed. The effects of temperature and confining pressure variations on fracture flow and permeability are being assessed as well, using relevant fractured samples from both SURF and the Milford Utah FORGE site. Frash et al. (2019) measure multiple geomechanical and hydrological properties of the Poorman schist using a triaxial direct-shear method (Figure 13). Integrated real-time X-ray imaging provides measurement of: 1) pre-shear permeability, 2) natural fracture structure, 3) peak shear

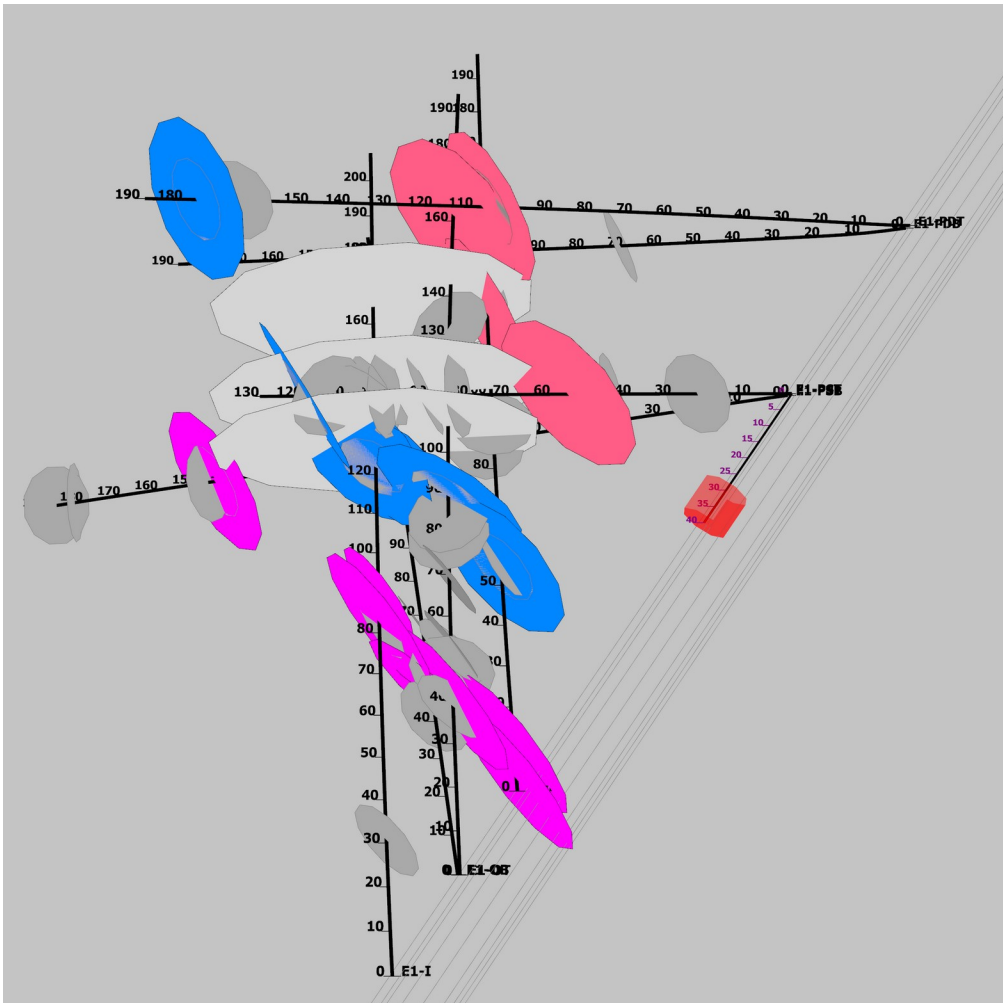

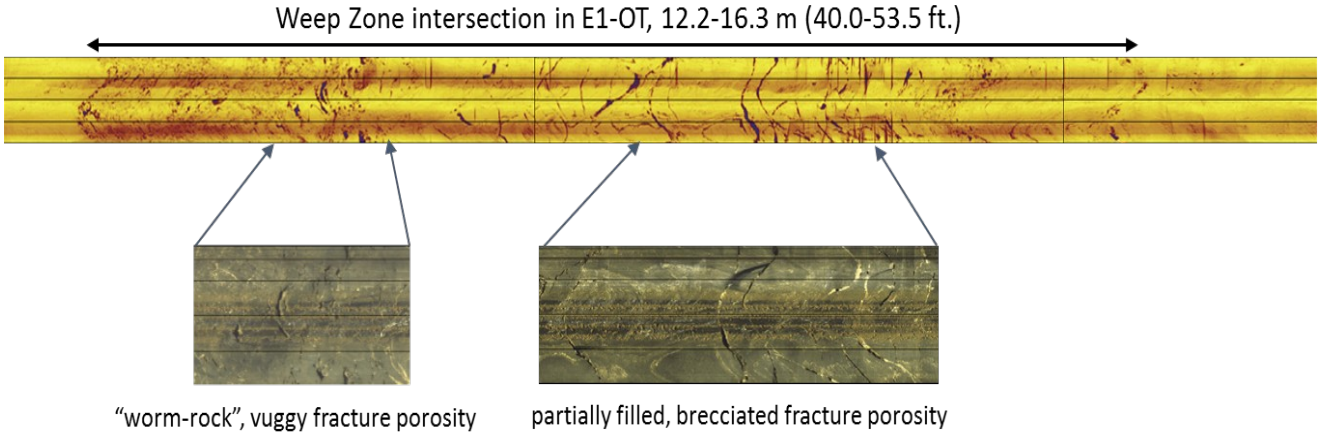

Figure 12. Top - Example of fractures incorporated in the CDFN shown in FracMan. Bottom – Acoustic and optical televiewer logs highlighting the observed weep zone.

strength, 4) residual shear strength, 5) hydroshear potential, 6) post-fracture permeability, 7) density, 8) acoustic velocity, 9) and shear-dilation angles. The experiments use 25 mm diameter by 25 mm length right-regular cylinder core plugs. From these experiments performed at actual site triaxial stress conditions, we have identified that natural foliation fractures containing graphite and/or aligned micas are the most likely features that could be hydroshear stimulated. We also find that the rock matrix permeability is very low, at less than 10 nD, which is less than previously expected.

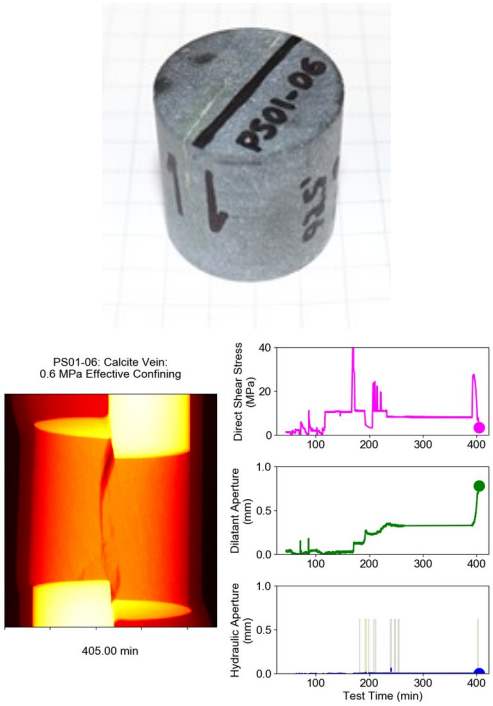

Figure 13. In-situ x-ray image and associated data from a triaxial direct shear test to quantify geomechanical and hydrological properties of the Poorman schist in the Experiment 1 test bed. From these tests, we find that the in-situ calcite-infilled natural fractures are nearly as strong as the matrix and can have very low permeability but that hydroshear is possible after they are disturbed, such as by hydraulic fracture stimulation.

Ye et al. (2019) performed laboratory true-triaxial and triaxial injection tests on an intact rock and a discontinuity (schistosity plane) of the Poorman Schist from the EGS Collab Experiment 1 site to characterize their failure behavior and fluid flow in response to injection (Figure 14). In the true-triaxial-injection test on the intact sample PS-IN1, pressurized gas permeated into a shear zone formed in the fine-grained foliation plane of the sample from a drilled wellbore. The induced micro-cracking and the resulting shearing zone coalesced and joined a shallow dipping mineralization band near the top of the sample. The resulting pore pressure increase facilitated slip failure in the shallower zone. The sequence of events is observed in the time evolution of the AE events distribution. The location of the recorded AE events and CT scanning images also indicate the deformation/shearing of the foliation plane. These observations demonstrate that the foliation plays an important role in the failure behavior and transport properties of Poorman schist during the hydraulic stimulation. For the sample with a major schistosity plane, PS-NF2, a triaxial-injection test with acoustic emission was carried out to focus on the seismo-hydro-mechanical response of the discontinuity and the associated permeability evolution during dilatant fracture shearing by injection. The results show that the stressed fracture can be sheared at injection pressure below the minimum principal stress, which matched with the concept of shear stimulation or hydroshearing. Upon shear slip, the fracture demonstrated normal dilation and was propped open, resulting in significant enhancement of flow rate/fracture permeability. In addition, the recorded microseismic events directly correlate with fracture shear slip and stress relaxation. Moreover, we proposed a systematic experimental workflow to characterize fracture properties, allowing us to achieve determination of a number of geomechanical properties from a single fracture. The characterized discontinuity properties, including stiffness, friction, shear strength, and stress-dependent permeability, can provide useful parameters for numerical modeling and field test interpretations.

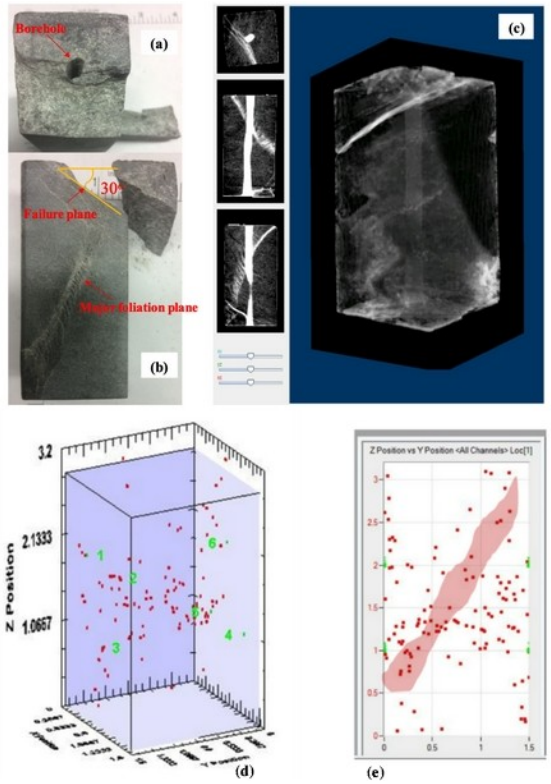

Figure 14: Failed sample PS-IN1 after the true-triaxial-injection test, (a) top view; (b) side view; (c) CT scanning images, (e) 3D location map of the microseismic events; (f) 2D sketch location map of the microseismic events.

8. DATA MANAGEMENT AND CURATION

EGS Collab data sets are curated on a secure collaboration space where DOE and EGS Collab partners have access to the data for research and model development (Weers et al., 2018; Weers and Huggins, 2019). This collaboration space provides an opportunity for project partners to help refine the data, ensuring quality prior to public release. Some large and high

bandwidth data sets are handled differently however, because these data streams reach nearly 2 Tb/day. Limited internet connectivity, due in part to the project's location nearly a mile underground, has required the EGS Collab team to prioritize data being transmitted out of the mine to assist with near-real-time decision making. The EGS Collab team is using edge processing in the mine to expose as much information as possible through the limited bandwidth available. For example, servers located in the mine process raw DTS data into simple plots that can be live broadcast from the mine during critical experiments (Weers and Huggins, 2019). Ultimate curation of the raw data for some of the larger datasets is not yet certain. Eventually, all data collected by the EGS Collab project will be made available to the public through the DOE Geothermal Data Repository.

9.0 Concluding Statements and Lessons Learned

9. CONCLUDING STATEMENTS AND LESSONS LEARNED

A significant amount of work has gone into predicting, planning, constructing, and executing EGS Collab tests to date and a significant amount of work analyzing data has begun. A diverse and talented group in the field, office, and laboratory carefully thought through many possible options, events, features, and processes, and created many conceptual and numerical models. High-quality data have been collected and are being collected and analyzed to interpret observations made during our tests. The numerical simulation teams have been developing conceptual and numerical of the hydrologic system of the testbed, and these models will be challenged with data to understand what happened, and to validate and improve the models.

Success in the EGS Collab project is in achieving scientific goals, therefore collecting lessons learned is very important and will be included in project papers. These include understanding the precision of measurements needed for the analyses required. Instrument location errors occur from simple measurement errors along a conveyance pipe, nonuniform conveyance pipe lengths, and very small angle errors in the orientation of the boreholes affect data interpretation. Simple location registration errors are common as many logging techniques, drillers, and researchers may use different fiducial marks as their datum, and the cables conveying these instruments may vary slightly from run to run. This problem is not unique to EGS Collab.

The EGS Collab has completed stimulations connecting our injection and production boreholes and collected high-quality data using numerous techniques. Tracer and thermal testing have been applied to understand flow properties. Many simulations have been performed and compared to data in an effort to improve modeling concepts and tools. Many unexpected things have occurred including obtaining different flow conditions while applying the same initial conditions, showing the nonlinearity of our systems. Our testbed was expected to be fracture-poor based on vertical coring, however many natural fractures have been observed in our subhorizontal boreholes.

10. ACKNOWLEDGMENTS

This material was based upon work supported by the U.S. Department of Energy, Office of Energy Efficiency and Renewable Energy (EERE), Office of Technology Development, Geothermal Technologies Office, under Award Number DE-AC02-05CH11231 with LBNL and other awards with other national laboratories. The

 We thank the drillers of Agapito Associates, Inc., for their skill and dedicated efforts to create our test bed boreholes. The research supporting this work took place in whole or in part at the Sanford Underground Research Facility in Lead, South Dakota. The assistance of the Sanford Underground Research Facility and its personnel in providing physical access and general logistical and technical support is gratefully acknowledged. The earth model output for this paper was generated using Leapfrog Software.

11. REFERENCES

1. Abass, H.H., S. Hedayati, and D.L. Meadows (1996), Nonplanar Fracture Propagation From a Horizontal Wellbore: Experimental Study, *SPE Production and Facilities*, *August*, 133-137, doi:10.2118/24823-PA.

2. Ajo-Franklin, J.B., T.M. Daley, B. Butler-Veytia, J. Peterson, Y. Wu, B. Kelley, and S. Hubbard (2011), Multi-level continuous active source seismic monitoring (ML-CASSM) : Mapping shallow hydrofracture evolution at a TCE contaminated site, in *Society of Exploration Geophysicists Annual Meeting*, edited.

3. Augustine, C. (2016), Update to Enhanced Geothermal System Resource Potential Estimate, *GRC Transactions*, *40*, 6.

4. Caddey, S.W., R.L. Bachman, T.J. Campbell, R.R. Reid, and R.P. Otto (1991), The Homestake gold mine, an early Proterozoic iron-formation-hosted gold deposit, Lawrence County, South Dakota, *Report Rep. 1857J*.

5. Chen, Y., L. Huang, J. Ajo-Franklin, T.J. Kneafsey, and E.C. Team (2018a), Toward Real-Time Microearthquake Event Detection and Location in Anisotropic Media Using a Multiscale Approach for EGS Collab Experiments, paper presented at Geothermal Resources Council 2018 Annual Meeting Geothermal Resources Council Transactions, Reno, NV.

6. Chen, Y., L. Huang, M. Schoenball, J. Ajo-Franklin, T. Kneafsey, and E.C. Team (2019), Real-Time Microearthquake Event Detection and Location in Anisotropic Media Using a Multiscale Scanning Approach for EGS Collab Experiments in *44th Workshop on Geothermal Reservoir Engineering*, edited, Stanford University, Stanford, California.

7. Chen, Y., L. Huang, and E.C. Team (2018b), Microearthquake Hypocenter-Location and Focal-Mechanism Inversions for the EGS Collab Project: A Synthetic Study, in *Proceedings, 43rd Workshop on Geothermal Reservoir Engineering*, edited, Stanford University, Stanford, CA.

8. Chen, Y., L. Huang, and E.C. Team (2018c), Microseismic Moment-Tensor Inversion for the EGS Collab Project: A Synthetic Study, in *PROCEEDINGS, 43rd Workshop on Geothermal Reservoir Engineering*, edited, Stanford University, Stanford, California.

9. Condon, K., H. Sone, and H.F. Wang (2018), Influence of Foliation Orientation on Rock Strength and Elastic Properties of Poorman Schist from the EGS Collab Experiment 1 Site, H11Q-1693 in *2018 AGU Fall Meeting*, edited, Washington, D.C.

10. Daley, T., B. Freifeld, J. Ajo-Franklin, S. Dou, R. Pevzner, V. Shulakova, S. Kashikar, D. Miller, J. Goetz, J. Henninges, and S. Lueth (2013), Field testing of fiber-optic distributed acoustic sensing (DAS) for subsurface seismic monitoring, *The Leading Edge*, *32*(6), 699-706, doi:10.1190/tle32060699.1.

11. Daley, T., R. Solbau, J. Ajo-Franklin, and S. Benson (2007), Continuous active-source seismic monitoring of C O2 injection in a brine aquifer, *GEOPHYSICS*, *72*(5), A57-A61, doi:10.1190/1.2754716.

12. Dobson, P., T. Kneafsey, J. Morris, A. Singh, M. Zoback, W. Roggenthen, T. Doe, G. Neupane, R. Podgorney, H. Wang, H. Knox, P. Schwering, D. Blankenship, C. Ulrich, T. Johnson, M. White, and E.C. team (2018), The EGS Collab Hydroshear Experiment at the Sanford Underground Research Facility – Siting Criteria and Evaluation of Candidate Sites, paper presented at Geothermal Resources Council 2018 Annual Meeting Geothermal Resources Council Transactions, Reno, NV.

13. Dobson, P., T.J. Kneafsey, D. Blankenship, C. Valladao, J. Morris, H. Knox, P. Schwering, M. White, T. Doe, W. Roggenthen, E. Mattson, R. Podgorney, T. Johnson, J. Ajo-Franklin, and E.C. Team (2017), An Introduction to the EGS Collab Project in *GRC Transactions, Vol. 41, 2017*, edited.

14. Doe, T.W., R. McLaren, and W. Dershowitz (2014), Discrete Fracture Network Simulations of Enhanced Geothermal Systems, in *39th Workshop on Geothermal Reservoir Engineering*, edited, p. 11, Stanford University.

15. El Rabaa, W. (1989), Experimental Study of Hydraulic Fracture Geometry Initiated From Horizontal Wells, in *64th Annual Technical Conference and Exhibition of the Society of Petroleum Engineers*, edited, Society of Petroleum Engineers, San Antonio, TX, doi:10.2118/19720-MS.

16. Frash, L.P., K. Arora, Y. Gan, M. Lu, M. Gutierrez, P. Fu, J. Morris, J. Hampton, and E.C. Team (2018a), Laboratory Validation of Fracture Caging for Hydraulic Fracture Control, in *52nd U.S. Rock Mechanics/Geomechanics Symposium*, edited, p. 8, American Rock Mechanics Association, Seattle, Washington.

17. Frash, L.P., J.W. Carey, N.J. Welch, and E.C. Team (2019), EGS Collab Experiment 1: Geomechanical and Hydrological Properties by Triaxial Direct Shear, in *44th Workshop on Geothermal Reservoir Engineering*, edited, Stanford University, Stanford, California.

18. Frash, L.P., P. Fu, J. Morris, and C.T. EGS (2018b), Fracture Caging: Can We Control the Extent of a Hydraulic Fracture Stimulated Zone?, paper presented at Proceedings, 43rd Workshop on Geothermal Reservoir Engineering, Stanford University, SGP-TR-213.

19. Fu, P., M. Schoenball, J. Morris, J. Ajo-Franklin, H. Knox, T. Kneafsey, J. Burghardt, M. White, and E.C. Team (2019), Microseismic Signatures of Hydraulic Fracturing: A Preliminary Interpretation of Intermediate-Scale Data from the EGS Collab Experiment, in *44th Workshop on Geothermal Reservoir Engineering*, edited, Stanford University, Stanford, California.

20. Fu, P., M. White, J. Morris, T. Kneafsey, and E.C. Team (2018), Predicting Hydraulic Fracture Trajectory Under the Influence of a Mine Drift in EGS Collab Experiment I, in *PROCEEDINGS, 43rd Workshop on Geothermal Reservoir Engineering*, edited, Stanford University, Stanford, California.

21. Gao, K., L. Huang, B. Chi, J. Ajo-Franklin, and E.C. Team (2018), Imaging the Fracture Zone Using Continuous Active Source Seismic Monitoring for the EGS Collab Project: A Synthetic Study,, in *PROCEEDINGS, 43rd Workshop on Geothermal Reservoir Engineering*, edited, Stanford University, Stanford, California.

22. Guglielmi, Y., F. Cappa, J.-P. Avouac, P. Henry, and D. Elsworth (2015), Seismicity triggered by fluid injection–induced aseismic slip, *Science*, *348*(6240), 1224.

23. Guglielmi, Y., F. Cappa, H. Lançon, J.B. Janowczyk, J. Rutqvist, C.F. Tsang, and J.S.Y. Wang (2013), ISRM Suggested Method for Step-Rate Injection Method for Fracture In-Situ Properties (SIMFIP): Using a 3-Components Borehole Deformation Sensor, in *The ISRM Suggested Methods for Rock Characterization, Testing and Monitoring: 2007–2014*, edited by R. Ulusay, Springer-Verlag, Wein, doi:DOI: 10.1007/978-3-319-07713-0.

24. Hart, K., T.C. Trancynger, W. Roggenthen, and J. Heise (2014), Topographic, geologic, and density distribution modeling in support of physics experiments at the Sanford Underground Research Facility (SURF), *Proceedings of the South Dakota Academy of Science*, *93*, 33-41.

25. Heise, J. (2015), The Sanford Underground Research Facility at Homestak, *Journal of Physics: Conference Series*, *606*(1), 26.

26. Huang, H., G.H. Neupane, R. Podgorney, E. Mattson, and E.C. Team (2019), Mechanistically Modeling of Hydraulic Fracture Propagation and Interaction with Natural Fractures at EGS-Collab Site in *44th Workshop on Geothermal Reservoir Engineering*, edited, Stanford University, Stanford, California.

27. Huang, L., Y. Chen, K. Gao, P. Fu, J. Morris, J. Ajo-Franklin, S. Nakagawa, and E.C. Team (2017), Numerical Modeling of Seismic and Displacement-Based Monitoring for the EGS Collab Project in *GRC Transactions, Vol. 41, 2017* edited.

28. Ingraham, M.D., D.K. King, H.A. Knox, C.E. Strickland, V.R. Vermeul, Y. Guglielmi, P. Cook, T. Doe, and E.C. Team (2018), Design of a long term hydraulic fracture and flow system, in *52nd US Rock Mechanics / Geomechanics Symposium*, edited, Seattle, Washington, USA, doi:ARMA 18–0130.

29. Johnson, T., C., R. Versteeg, J., F. Day-Lewis, D., W. Major, and L.J. W. (2014), Time-Lapse Electrical Geophysical Monitoring of Amendment-Based Biostimulation, *Groundwater*, *53*(6), 920-932, doi:10.1111/gwat.12291.

30. Johnson, T., C. Strickland, H. Knox, J. Thomle, V. Vermuel, C. Ulrich, T. Kneafsey, D. Blankenship, and E.C. Team (2019), EGS Collab Project Electrical Resistivity Tomography Characterization and Monitoring Status, in *44th Workshop on Geothermal Reservoir Engineering*, edited, Stanford University, Stanford, California.

31. Kneafsey, T.J., P. Dobson, D. Blankenship, J. Morris, H. Knox, P. Schwering, M. White, T. Doe, W. Roggenthen, E. Mattson, R. Podgorney, T. Johnson, J. Ajo-Franklin, C. Valladao, and E.C. team (2018a), An Overview of the EGS Collab Project: Field Validation of Coupled Process Modeling of Fracturing and Fluid Flow at the Sanford Underground Research Facility, Lead, SD in *PROCEEDINGS, 43rd Workshop on Geothermal Reservoir Engineering*, edited, Stanford University, Stanford, California.

32. Kneafsey, T.J., P.F. Dobson, J.B. Ajo-Franklin, C. Valladao, D.A. Blankenship, H.A. Knox, P. Schwering, J.P. Morris, M. Smith, M.D. White, T. Johnson, R. Podgorney, E. Mattson, G. Neupane, W. Roggenthen, T. Doe, and E.C. team (2018b), The EGS Collab Project: Stimulation and Simulation, in *52nd US Rock Mechanics / Geomechanics Symposium held in , USA,* , edited, Seattle, Washington, USA.

33. Knox, H., P. Fu, J. Morris, Y. Guglielmi, V. Vermeul, J. Ajo-Franklin, C. Strickland, T. Johnson, P. Cook, C. Herrick, M. Lee, and E.C. Team (2017), Fracture and Flow Designs for the Collab/Sigma-V Project in *GRC Transactions, Vol. 41, 2017* edited.

34. Knox, H.A., Ajo-Franklin, J., Johnson, T.C., Morris, J.P., Grubelich, M.C., Preston, L.A., , J.M. Knox, and D. King (2016), High energy stimulations imaged with geophysical change detection techniques., in *Geothermal Resources Council Transactions*, edited, p. 11.

35. Linneman, D., H. Knox, P. Schwering, and C.R. Hoots (2018), The EGS Collab Hydrofracture Experiment at the Sanford Underground Research Facility – Campaign Cross-Borehole Seismic Characterization, H11Q-1689, in *AGU Fall Meeting*, Washington, D.C.

36. Lu, J., and A. Ghassemi (2019), Coupled THMS Modeling of Fractured Reservoir Stimulation with Application to EGS Collab, in *44rd Workshop on Geothermal Reservoir Engineering*, edited, Stanford University, Stanford, California.

37. Mattson, E., M. White, Y. Zhang, B. Johnston, A. Hawkins, and E.C. Team (2018), Collab Fracture Characterization: Preliminary Results from the Modeling and Flow Testing of Experiment 1, paper presented at Geothermal Resources Council 2018 Annual Meeting Geothermal Resources Council Transactions, Reno, NV.

38. Mattson, E., Y. Zhang, A. Hawkins, T. Johnson, J. Ajo-Franklin, G. Neupane, and E.C. Team (2019), Preliminary Collab Fracture Characterization Results from Flow and Tracer Testing Efforts in *44th Workshop on Geothermal Reservoir Engineering*, edited, Stanford University, Stanford, California.

39. Morris, J.P., P. Dobson, H. Knox, J. Ajo-Franklin, M.D. White, P. Fu, J. Burghardt, T.J. Kneafsey, D. Blankenship, and E.C. Team (2018a), Experimental Design for Hydrofracturing and Fluid Flow at the DOE Collab Testbed in *PROCEEDINGS, 43rd Workshop on Geothermal Reservoir Engineering*, edited, Stanford University, Stanford, California.

40. Morris, J.P., P. Fu, P. Dobson, J. Ajo-Franklin, T.J. Kneafsey, H. Knox, D. Blankenship, M.D. White, J. Burghardt, T.W. Doe, and E.G.S.C. Team (2018b), Experimental Design for Hydrofracturing and Fluid Flow at the DOE EGS Collab Testbed, in *52nd U.S. Rock Mechanics/Geomechanics Symposium*, edited, p. 11, American Rock Mechanics Association, Seattle, Washington.

41. Newman, G., and P. Petrov (2018), Seismic Source Mechanism Estimation in 3D Elastic Media, in *PROCEEDINGS, 43rd Workshop on Geothermal Reservoir Engineering*, edited, Stanford University, Stanford, California.

42. Oldenburg, C.M., P.F. Dobson, Y. Wu, P.J. Cook, T.J. Kneafsey, S. Nakagawa, C. Ulrich, D.L. Siler, Y. Guglielmi, J. Ajo-Franklin, J. Rutqvist, T.M. Daley, J.T. Birkholzer, H.F. Wang, N.E. Lord, B.C. Haimson, H. Sone, P. Vigilante, W.M. Roggenthen, T.W. Doe, M.Y. Lee, M. Ingraham, H. Huang, E.D. Mattson, J. Zhou, T.J. Johnson, M.D. Zoback, J.P. Morris, J.A. White, P.A. Johnson, D.D. Coblentz, and J. Heise (2017), Hydraulic fracturing experiments at 1500 m depth in a deep mine: Highlights from the kISMET project, in *42nd Workshop on Geothermal Reservoir Engineering*, edited, p. 9, Stanford University.

43. Pan, W., L. Huang, K. Gao, J. Ajo-Franklin, T.J. Kneafsey, and E.C. Team (2019), Anisotropic Full-Waveform Inversion and Least-Squares Reverse-Time Migration of CASSM Data for Experiment I of the EGS Collab Project in *44th Workshop on Geothermal Reservoir Engineering*, edited, Stanford University, Stanford, California.

44. Roggenthen, W.M., and T.W. Doe (2018), Natural Fractures and Their Relationship to the EGS Collab Project in the Underground of the Sanford Underground Research Facility (SURF), in *52nd U.S. Rock Mechanics/Geomechanics Symposium*, edited, p. 11, American Rock Mechanics Association, Seattle, Washington.

45. Schoenball, M., J. Ajo-Franklin, D. Blankenship, P. Cook, P. Dobson, Y. Guglielmi, P. Fu, T. Kneafsey, H. Knox, P. Petrov, M. Robertson, P. Schwering, D. Templeton, C. Ulrich, T. Wood1, and E.C. Team (2019), Microseismic monitoring of meso-scale stimulations for the DOE EGS Collab project at the Sanford Underground Research Facility, in *44th Workshop on Geothermal Reservoir Engineering*, edited, Stanford University, Stanford, California.

46. Schwering, P.C., D. Blankenship, R.K Podgorney, G.H. Neupane, T. Doe, C. Ulrich, P.F. Dobson, T.J. Kneafsey, A. Singh, M.M. Smith, W. Roggenthen, N. Uzunlar, and EGS Collab Team (2018), The First EGS Collab Testbed at the Sanford Underground Research Facility – Discrete Fracture Network Characterization, 2018 AGU Fall Meeting, H32C-06.

47. Schwering, P.C., H.A. Knox, C.R. Hoots, D. Linneman, J. Ajo-Franklin, and E.C. team (2018), The EGS Collab Hydrofracture Experiment at the Sanford Underground Research Facility – Campaign Cross-Borehole Seismic Characterization, paper

presented at Geothermal Resources Council 2018 Annual Meeting Geothermal Resources Council Transactions, Reno, NV, October 14-17, 2018.

48. Templeton, D., J. Morris, M. Schoenball, T. Wood, M. Robertson, P. Cook, P. Dobson, C. Ulrich, J. Ajo-Franklin, T. Kneafsey, P. Schwering, D. Blankenship, H. Knox, and E.C. Team (2019), Microseismic Correlation and Cluster Analysis of DOE EGS Collab Data, in *44th Workshop on Geothermal Reservoir Engineering*, edited, Stanford University, Stanford, California.

49. Ulrich, C., P.F. Dobson, T.J. Kneafsey, W.M. Roggenthen, N. Uzunlar, T.W. Doe, G. Neupane, R. Podgorney, P. Schwering, L. Frash, and A. Singh (2018), The Distribution, Orientation, and Characteristics of Natural Fractures for Experiment 1 of the EGS Collab Project, Sanford Underground Research Facility, in *52nd U.S. Rock Mechanics/Geomechanics Symposium*, edited, p. 8, American Rock Mechanics Association, Seattle, Washington.

50. Wang, H.F., M.Y. Lee, T.W. Doe, B.C. Haimson, C.M. Oldenburg, and P.F. Dobson (2017), In-Situ Stress Measurement at 1550-Meters Depth at the kISMET Test Site in Lead, S.D, in *51st U.S. Rock Mechanics/Geomechanics Symposium*, edited, American Rock Mechanics Association, San Francisco, California, USA.

51. Weers, J., J. Ajo-Franklin, and J. Huggins (2019), Getting Data Out of the Ground: Modern Challenges Facing EGS Collab, the DOE Geothermal Data Repository, and the Geothermal Industry, in *44th Workshop on Geothermal Reservoir Engineering*, edited, Stanford University, Stanford, CA.

52. Weers, J.D., H. Johnston, and J.V. Huggins (2018), The EGS Data Collaboration Platform: Enabling Scientific Discovery, in *PROCEEDINGS, 43rd Workshop on Geothermal Reservoir Engineering*, edited, National Renewable Energy Lab.(NREL), Golden, CO (United States), Stanford University, Stanford, California, .

53. Weers, J., and J. Huggins (2019), Getting Data Out of the Ground: Modern Challenges Facing EGS Collab, the DOE Geothermal Data Repository, and the Geothermal Industry, in *44th Workshop on Geothermal Reservoir Engineering*, edited, Stanford University, Stanford, CA.

54. White, M., P. Fu, H. Huang, A. Ghassemi, and E.C. Team (2017), The Role of Numerical Simulation in the Design of Stimulation and Circulation Experiments for the EGS Collab Project in *GRC Transactions, Vol. 41, 2017* edited.

55. White, M., T. Johnson, T. Kneafsey, D. Blankenship, P. Fu, H. Wu, A. Ghassemi, J. Lu, H. Huang, G. Neupane, C. Oldenburg, C. Doughty, B. Johnston, P. Winterfeld, R. Pollyea, R. Jayne, A. Hawkins, Y. Zhang, and E.C. Team (2019), The Necessity for Iteration in the Application of Numerical Simulation to EGS: Examples from the EGS Collab Test Bed 1, in *44th Workshop on Geothermal Reservoir Engineering*, edited, Stanford University, Stanford, California.

56. White, M.D., P. Fu, A. Ghassemi, H. Huang, J. Rutqvist, B. Johnston, and E.C. Team (2018), Numerical Simulation Applications in the Design of EGS Collab Experiment 1, in *PROCEEDINGS, 43rd Workshop on Geothermal Reservoir Engineering*, edited, Stanford University, Stanford, California.

57. Williams, C.F., M.J. Reed, R.H. Mariner, J. DeAngelo, and S.P. Galanis, Jr. (2008), Assessment of moderate- and high-temperature geothermal resources of the United States, edited by U. S. G. Survey, p. 4.

58. Winterfeld, P., B. Johnston, K. Beckers, Y.-S. Wu, and E.C. Team (2019), Code Modifications for Modeling Chemical Tracers and Embedded Natural Fractures at EGS Collab, in *44th Workshop on Geothermal Reservoir Engineering*, edited, Stanford University, Stanford, California.

59. Wu, H., P. Fu, J.P. Morris, E.D. Mattson, A.J. Hawkins, Y. Zhang, R.R. Settgast, F.J. Ryerson, and E.C. Team (2019a), Characterizing Fracture Flow in EGS Collab Experiment Based on Stochastic Modeling of Tracer Recovery, in *44th Workshop on Geothermal Reservoir Engineering*, edited, Stanford University, Stanford, California.

60. Wu, H., P. Fu, J.P. Morris, R.R. Settgast, F.J. Ryerson, and E.C. Team (2019b), A Numerical Scheme to Reduce Numerical Diffusion for Advection-Dispersion Modeling: Validation and Application, in *44th Workshop on Geothermal Reservoir Engineering*, edited, Stanford University, Stanford, California.

61. Wu, H., P. Fu, X. Yang, J.P. Morris, and E.C. Team (2018), Imaging hydraulic fracture extents and aperture using electrical resistivity tomography, in *PROCEEDINGS, 43rd Workshop on Geothermal Reservoir Engineering*, edited, Stanford University, Stanford, California.

62. Ye, Z., A. Vachaparampil, X. Zhou, A. Ghassemi, and T. Kneafsey (2019), Failure Behavior of the Poorman Schist and Its Fractures from EGS Collab Stimulation Site, in *44th Workshop on Geothermal Reservoir Engineering*, edited, Stanford University, Stanford, California.

63. Yildirim, E.C., K. Im, and D. Elsworth (2018), Co-Evolution of Fracture Permeability and Friction in Rocks From the EGS Collab Experiment 1 Site, in *52nd U.S. Rock Mechanics/Geomechanics Symposium*, edited, p. 8, American Rock Mechanics Association, Seattle, Washington.

64. Zang, A., O. Stephansson, L. Stenberg, K. Plenkers, S. Specht, C. Milkereit, E. Schill, G. Kwiatek, G. Dresen, G. Zimmermann, T. Dahm, and M. Weber (2017), Hydraulic fracture monitoring in hard rock at 410 m depth with an advanced fluid-injection protocol and extensive sensor array, *Geophysical Journal International*, 790–813, doi:10.1093/gji/ggw430.

65. Zhang, Y., C. Doughty, L. Pan, T. Kneafsey, and E.C. Team (2018a), What Could We See at the Production Well Before the Thermal Breakthrough?, in *PROCEEDINGS, 43rd Workshop on Geothermal Reservoir Engineering*, edited, Stanford University, Stanford, California.

66. Zhang, Y., Q. Zhou, S. Finsterle, T. Kneafsey, R. Jayne, and E.C. Team (2018b), Thermal breakthrough predictions based on multiple flow paths characterized by tracer tests, in *TOUGH Symposium*, edited, Lawrence Berkeley National Laboratory. Berkeley, California.

67. Zhou, Q., C.M. Oldenburg, T.J. Kneafsey, and E.C. Team (2018), Modeling Transport of Multiple Tracers in Hydraulic Fractures at the EGS Collab Test Site, in *PROCEEDINGS, 43rd Workshop on Geothermal Reservoir Engineering*, edited, Stanford University, Stanford, California.